Supplemental Figures

Figure S1 (related to Figure 1)

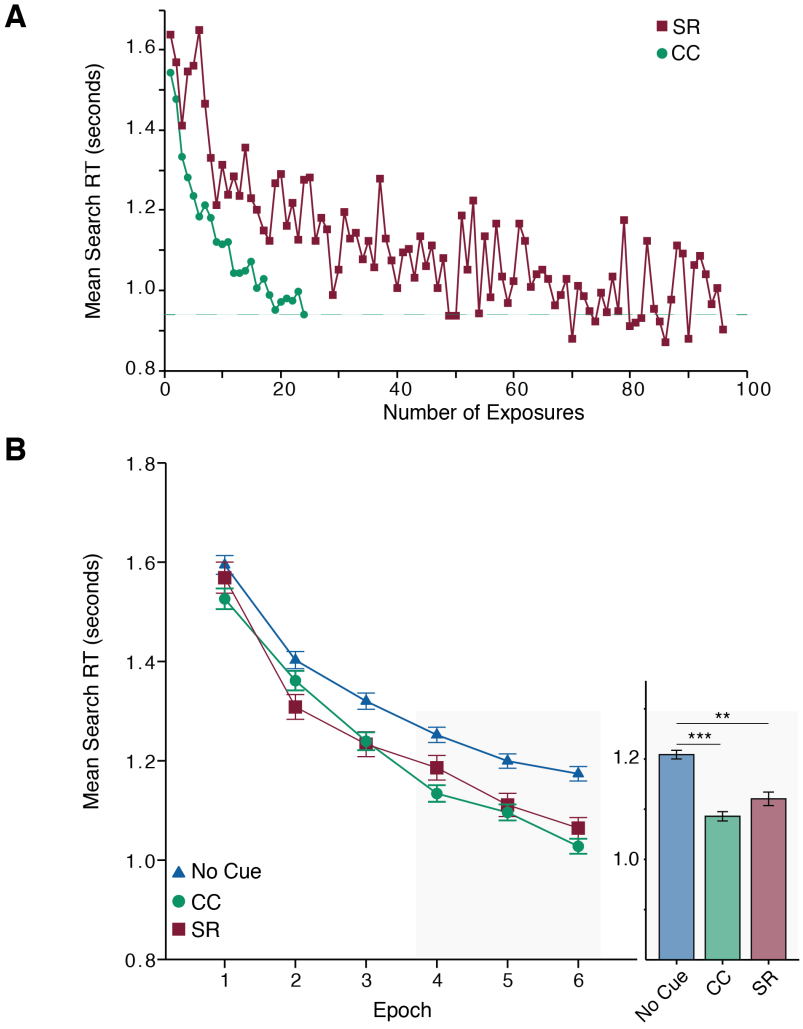

Figure S1: Time course and replication of memory-guided attention
(A) Participants needed many more exposures to show attentional benefits from stimulus-response (SR) compared to context (CC) associations. Data shown are averaged across all participants (N = 35). The dashed green line shows the minimum reaction time (RT), on average, achieved on CC trials.
(B) In an independent sample (N = 42) collected outside the MRI scanner, participants were significantly faster at finding the target in the presence of context (CC) or stimulus-response (SR) cues than no cue ($F(2,82) = 6.41$, $p = .005$). One epoch = average of four sequential blocks (directly comparable to Fig. 1d). There was no significant difference in reaction time between CC and SR trials. In the second half of the experiment, participants were significantly faster on CC ($t(41) = 5.66$, $p < .001$) and SR ($t(41) = 3.24$, $p = .002$) compared to No Cue trials. RT = reaction time. Error bars = 1 SE. $^{**}p < .01$, $^{***}p < .001$.

Figure S2 (related to Figure 1, Experimental Procedures)

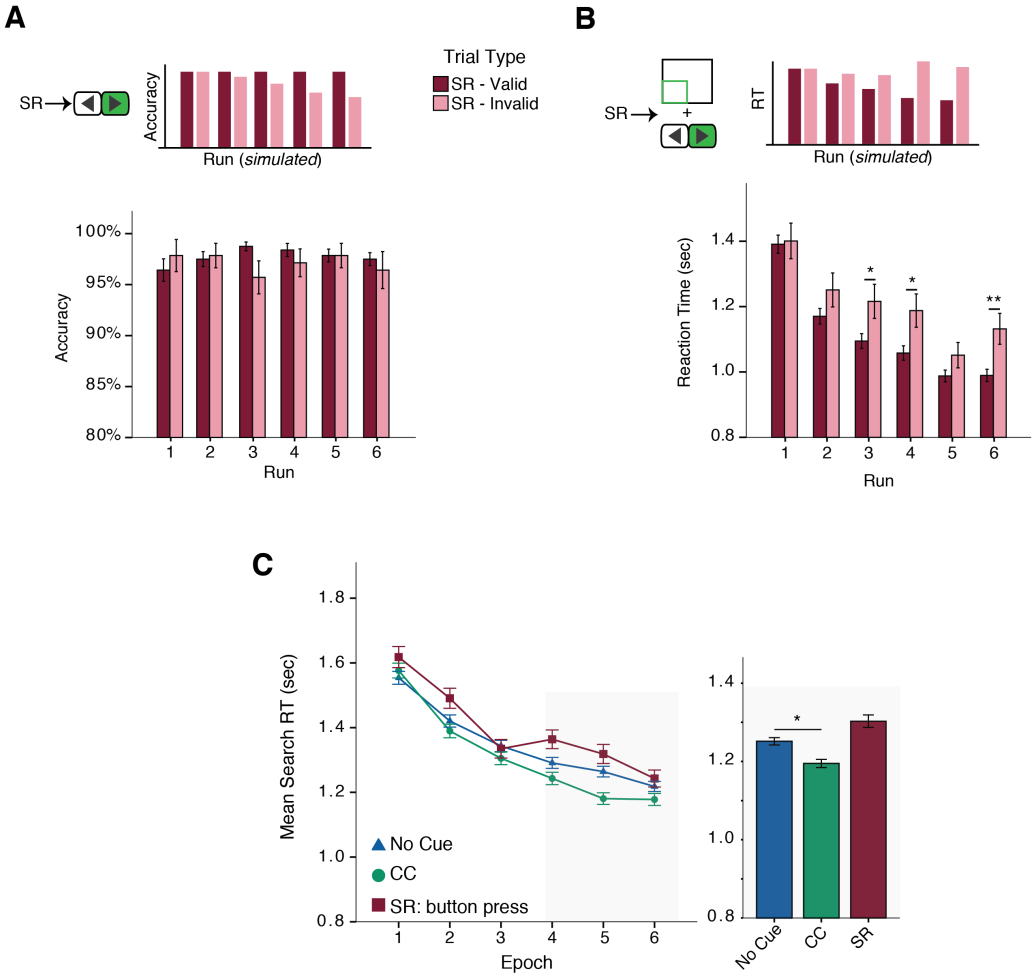

Figure S2: Stimulus-response associations involve more than button press response
It is possible that the performance benefit on stimulus-response trials was due to the stimulus simply cueing the button-press response, with no influence on attention. This can be tested by comparing SR-valid to SR-invalid trials (as the SR-association was only 80% valid). While both trial types share the same stimulus (shape color), the SR-valid button-press and "T" location were incorrect on SR-invalid trials.
(A) If participants simply performed the button-press response in the presence of the stimulus, accuracy for SR-invalid trials (pink) should decrease relative to SR-valid trials (red) as participants learned the SR-valid association (schematic, top). However, there was no significant difference in accuracy between SR-valid and SR-invalid trials at any point during the experiment, suggesting that participants did not simply perform the button-press response in the presence of the stimulus (bottom).
(B) If, however, participants learned something that guided their attention as well as cued the button-press response, reaction time (RT) should increase on SR-invalid relative to SR-valid trials as participants learned the SR-valid association (schematic, top). This pattern was observed in the data (bottom, accurate trials only).
(C) To further demonstrate that SR-associations cue more than a button-press, we conducted a follow-up study in which the SR association only cued the button press response. A new cohort of 35 participants completed the task, with an additional three being excluded due to error rates >15%. Participants did not show faster reaction times on SR trials than on trials with No Cue, showing that this association was not sufficient to change performance. However, contextual cueing still facilitates performance: we observed a type x epoch interaction when comparing CC to No Cue trials ($F(5,170) = 2.69$, $p < .05$) and participants were significantly faster on CC than No Cue trials during the second half ($t(34) = 2.6$, $p < .05$). *$p < .05$, **$p < .01$.

Figure S3 (related to Figure 3, Table 1)

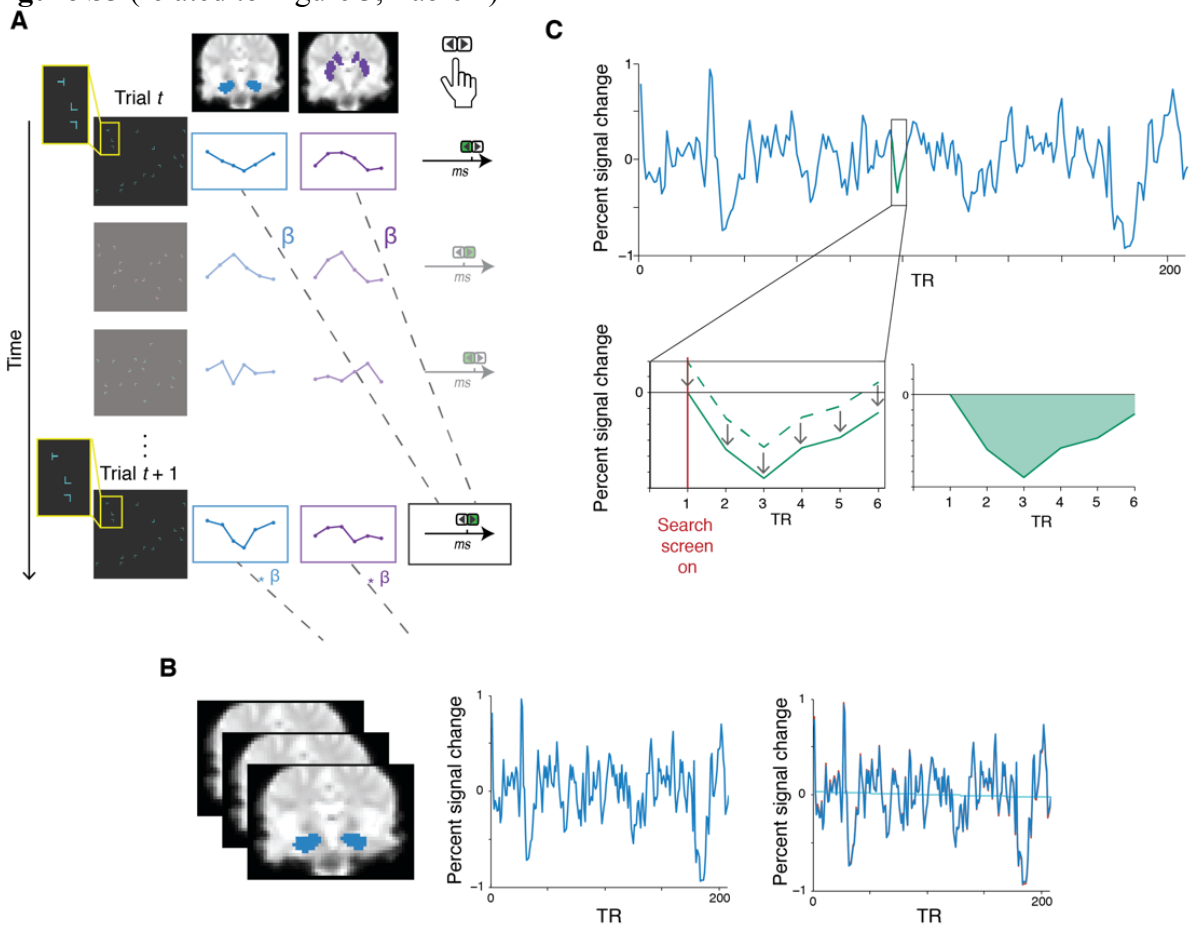

Figure S3: Computing the subsequent attention effect

(A) Schematic of subsequent attention effect analysis. For every trial *t*, we computed the trial-evoked response averaged across voxels in the hippocampus and striatum (regions of interest, ROIs), and recorded the participant's reaction time. We used the trial-evoked response in each ROI to predict the reaction time on trial *t+1*. We conducted this analysis separately for context cued (as shown in schematic) and stimulus-response cued trials, enabling us to determine the extent to which signal in each ROI related to trial-by-trial variability in performance. This approach is analogous to the subsequent memory effect (Wagner et al), in that neural activity on trial *t* is used to predict behavior on trial *t+1*.
(B, C) To compute the trial-evoked response, we adapted methods from (Dinstein et al., 2012). These responses were used both to predict subsequent behavior (Figure 3a-c) and neural activity (Figure 3d-e).
(B) For each subject, we aligned each run to the subject's calibration scan. We also aligned each anatomically defined ROI to the calibration scan, providing a map of ROI voxels for each functional run (left panel). For each voxel in each ROI, we extracted the fMRI time-course throughout the experiment. We divided the time-course by the mean to account for distance from the RF coil and convert to percent signal change (center panel). Any outlier time-points (>5 standard deviations outside the mean percent signal change in the ROI) were replaced by the average of two time-points pre and post-outlier. We then subtracted the best-fit line (light blue) from the time series (red) to remove effects of drift and trend (updated time-series shown in blue, right panel). No further pre-processing was conducted.
(C) We segmented these corrected time-courses into six-TR (12 sec) epochs starting at stimulus onset (dashed line), setting the signal at stimulus onset to zero (solid line). As we expected the hemodynamic response to have slightly different shapes in each ROI, we chose to compute the area under the curve for the full epoch rather than selecting particular time-points to reflect the trial-evoked response (as done by Dinstein and colleagues). Area under the curve was computed using Eq 3 (area under the curve with respect to ground) from Preussner and colleagues (Pruessner et al., 2003).

Table S1. Common activations in memory (context and stimulus-response) and visually-guided search. (Related to Figure 3)

Brain Region	X	Y	Z	*p* value
Frontal				
R anterior insula	34	20	0	$p < .001$
	38	16	2	$p < .001$
L anterior insula	-28	20	0	$p < .001$
	-34	14	2	$p < .001$
L central opercular cortex	-44	-4	8	$p = .047$
R precentral gyrus	52	10	22	$p < .001$
	44	6	22	$p < .001$
	46	2	50	$p = .012$
	44	0	54	$p = .009$
	38	-2	42	$p < .001$
L precentral gyrus	-56	6	30	$p < .001$
	-56	6	20	$p = .027$
	-40	4	28	$p < .001$
	-52	4	32	$p < .001$
	-44	2	28	$p < .001$
	-42	-6	42	$p = .021$
	-24	-10	44	$p < .001$
R anterior cingulate	8	20	34	$p < .001$
R paracingulate	6	16	40	$p = .005$
	8	12	46	$p = .048$
L paracingulate/anterior cingulate	-4	14	42	$p = .007$
	-8	10	42	$p = .002$
	-4	8	46	$p < .001$
R middle frontal gyrus/white matter	32	0	48	$p < .001$
L supplementary motor cortex	-4	4	48	$p < .001$
L superior frontal gyrus	26	-4	48	$p < .001$
Parietal				
R superior parietal lobule	34	-44	40	$p < .001$
	38	-50	46	$p < .001$
	32	-50	40	$p < .001$
L postcentral gyrus	-62	-16	22	$p = .004$
	-62	-18	30	$p = .015$
Temporal				
R posterior hippocampus	22	-30	-8	$p < .001$
L posterior hippocampus	-20	-30	-8	$p < .001$
Occipital				
R lateral occipital cortex	20	-74	50	$p < .001$
L lateral occipital cortex	-18	-74	42	$p < .001$
Subcortical				
R putamen	22	8	0	$p < .001$
R thalamus/white matter	14	-14	-4	$p < .001$
L thalamus/white matter	-6	-14	-6	$p < .001$
Brainstem	0	-36	-44	$p < .001$
Cerebellum				
Vermis	2	-58	-40	$p < .001$
R cerebellar hemisphere	22	-36	-44	$p = .001$
L cerebellar hemisphere	-14	-64	-24	$p = .042$
	-16	-42	-42	$p < .001$

R = right hemisphere, L = left hemisphere. Table includes peak and local maxima. *P* values are Bonferroni corrected for multiple comparisons. Coordinates are in standard MNI atlas space.

Supplemental Experimental Procedures

Participants

Thirty-five right-handed participants (51% female, mean age=21.7) completed the study for monetary compensation. Three additional participants were excluded due to technical issues, claustrophobia, and falling asleep. All participants had normal or corrected-to-normal vision and normal color vision. All participants provided written informed consent in accordance with procedures approved by the New York University Committee on Activities Involving Human Subjects.

Task design

In the visual search task, participants searched for a target among distractors (Figure 1). The target was a "T" stimulus rotated 90° to the right or left, and the distractors were offset-"L" shapes (rotated 0°, 90°, 180°, or 270°). Participants were told to press one of two keys based on whether the bottom of the "T" pointed right or left. Each search screen contained 16 items positioned on an invisible 12x8 grid, distributed so that 4 items appeared in each quadrant. Configurations of target and distractors were randomly generated for each participant, and the SR-predictive color and cued response were randomly assigned. To increase the salience of the SR-predictive color, practice trials were not presented in this color. Stimuli were presented in blue (RGB 0 240 240) or pink (255 133 214), matched for luminance, against a gray background.

Participants first completed 24 practice trials, in which no mnemonic cues were present. Following the practice block, participants completed 576 trials, divided into 6 runs. They had four seconds to respond to each screen. Immediately after each response (or four seconds, whichever came first), the search screen disappeared. Mnemonic cues included repeated layouts (contextually cued, CC) or probabilistic stimulus-response (SR) associations. On CC trials, the spatial configuration of the display cued the precise location of the target. On SR trials, the stimulus color probabilistically cued the location of the target and the participant's motor response.

Each search screen was preceded by a fixation screen (jittered, mean 2 sec) with a small white dot at the center, and followed by a feedback screen (0.5 sec), displaying points earned during the preceding search. Points were calculated based on RT and accuracy, with 1-10 points received on accurate trials, 0 for missed trials, and -10 for incorrect responses. Total points earned were shown at the end of each block.

To reduce factors that might bias search, the "T" appeared equally often in each quadrant, at each distance from the fixation point, and facing either direction (eliciting each motor response equally). This caused the 24 trials in each block to be divided as follows: 8 unique CC configurations (two per quadrant), 4 SR, 1 INV ("invalid"— the SR cue (stimulus color) was present, but the SR response ("T" quadrant and pointing direction) was not correct, thus reducing the predictive validity of the SR cue to 80%), and 11 No Cue. To reduce RT variability, the "T" did not appear in the band of eccentricity nearest to or farthest from fixation. As in earlier studies, to control for effects due to repetition of target location, there were 24 possible target locations (distributed across trial types) that

repeated in each block.

Immediately after search, participants completed two blocks testing explicit memory for contextual and stimulus-response associations. In the first block, following earlier studies (Chun and Jiang, 2003), participants viewed screens from which the "T" had been removed and replaced with a distractor. They were asked to indicate the quadrant in which the "T" appeared when they viewed the screen previously, providing a measure of explicit memory for CC and SR associations. In the second block, they were asked to recall the direction the "T" was pointing, probing explicit memory for SR associations.

Stimuli were presented using MATLAB (2012a; The MathWorks, Natick, MA) with the Psychophysics Toolbox extension (v3; Brainard, 1997). These were projected onto a screen at the back of the bore of the MRI magnet, viewed using a mirror attached to the head coil. Behavioral data were analyzed using SPSS (v22; IBM SPSS Statistics).

Event-related design: timing
We ran simulations of BOLD responses to determine timing of inter-trial intervals (ITIs), in order to enhance our ability to detect activity specific to each trial type. Using data from a previous pilot (Figure S1), we randomly selected five participants, using their reaction time on each trial to set the on and offset times of search screens (adding on 0.5 s for feedback screens). We then added ITIs between search screens, drawing from geometric, exponential, and Poisson distributions, following previous research showing the efficacy of long-tailed distributions for event related designs (Hagberg et al., 2001). All distributions had a mean duration of 2 seconds. Next, we convolved trial on and offsets from each trial type with a canonical hemodynamic response function, and reduced the resolution to 2 second TRs. We repeated this simulation process for a TR-locked design (in which every search screen was displayed at the beginning of a TR), and fixed-length trials (in which each trial–search screen + ITI–was equal to 3 TR).
We correlated the signal resulting from each trial type, and averaged this across the participants we used to create the simulations. In several iterations, the non-TR-locked design with ITIs drawn from a geometric distribution yielded the optimal design (minimal correlation between trial types).

fMRI data collection
The scanning session began with a high-resolution, T1-weighted anatomical scan (magnetization-prepared rapid-acquisition gradient echo sequence, 1x1x1mm voxels, TR=2500 ms, TE=3.93 ms, flip angle=8°) followed by a calibration scan. During the experiment, participants responded using a magnet-safe button box. After one block of practice, participants completed 6 runs of search (4 blocks each). As the duration of each run varied based on the participant's reaction time, the experimenter manually stopped each run. Each run began with 8 seconds of rest.

Functional images were acquired using a single-shot gradient echo EPI sequence (TR=2000 ms, TE=30 ms, FOV=240 cm, flip angle=82°). Thirty-five contiguous oblique-axial slices (3x3x3mm voxels) parallel to the AC/PC line were obtained.

fMRI analyses

Regions of interest

A priori regions of interest (ROIs) were defined anatomically per subject using FSL's FIRST (FMRIB's Integrated Registration and Segmentation Tool; (Patenaude et al., 2011)). We defined the striatum as bilateral caudate and putamen ((Poldrack and Packard, 2003); human homologues of the dorsolateral striatum, see (Yin and Knowlton, 2006)). Based on earlier studies of memory-guided attention indicating distinct roles of hippocampal subregions (Giesbrecht et al., 2013; Greene et al., 2007; Kasper et al., 2015; Summerfield et al., 2006), we separated the hippocampus into left, right, anterior, and posterior regions. To determine the latter two ROIs, we segmented each subject's hippocampus into three equidistant portions, using the most anterior and posterior thirds as ROIs (Staresina et al., 2011).

Image pre-processing

For all analyses, the first two volumes of each run were discarded to allow for signal normalization. Preprocessing used to derive the area under the curve for the subsequent attention effect analyses (Figure 3a-c) is described in Figure S4.
For the neural mechanism of the subsequent attention effect (Figure 3d) and the individual difference analyses (Figure 4), further preprocessing steps were conducted. Preprocessing included slice-time correction, motion correction, FSL's FILM pre-whitening algorithm, a high-pass temporal filter of 100s, and spatial smoothing with a Gaussian kernel of 5-mm full-width-at-half-maximum (FWHM). Functional images were aligned to brain-extracted high-resolution scans for each subject using boundary-based registration (Greve and Fischl, 2009). For group level analyses, images were linearly transformed (12 degrees of freedom) into MNI152 space.

General linear models

For all general linear models, we convolved a boxcar (initiating at stimulus onset and terminating at participant response) with a canonical HRF. We modeled trials using variable epoch durations (duration = RT) rather than impulses in order to improve statistical power (Grinband et al., 2008). General linear model analyses were conducted using FSL v5.0.4 (FMRIB's Software Library, www.fmrib.ox.c.uk/fsl). First level analyses were conducted in native space.

Subsequent attention effect: behavioral analyses

Trial-evoked responses were computed as described in Figure S4. Using linear regression, *z*-scored responses from each ROI on trial *t* were used to predict reaction time (RT, *z*-scored) on trial *t+1* (accurate trials only). We ran this analysis separately for CC and SR trials, deriving β values per ROI, per trial type, per participant. As there were eight unique CC configurations, we ran separate linear regressions for each configuration, then averaged across the configuration β values.

We ran two sets of linear regressions. In the first, we included signal from the hippocampus and striatum in the same model, enabling us to compare the strength of the association between signal in each ROI and RT on the subsequent trial (Figure 3b). In the second set, to determine whether these differences were driven by signal in specific

subregions within the ROIs we extracted signal from each subregion and then ran separate regressions in which only one region at a time served as a predictor (Figure 3c). Analyses were run in MATLAB.

Subsequent attention effect: neural mechanism

To probe the mechanism by which BOLD signal predicted subsequent reaction time, we set up a general linear model (GLM) to use BOLD signal to predict subsequent neural responses. We created one regressor each for accurate SR, No Cue, and Invalid Cue (SR color, but not SR response) trials, and eight CC regressors (one for each configuration). An additional Error nuisance regressor was included. For CC and SR trials, we created two additional regressors with hippocampal or striatal response (same AUC used in the SAE behavioral analysis) from the preceding trial as the parametric modulator.

To measure negative correlations with the hippocampus on CC trials (as decreased hippocampal signal predicted decreased RT), we weighted the 8 CC regressors with the hippocampal parametric modulator as -0.125. To measure positive correlations with the striatum on SR trials, we weighted the SR regressor with the striatal parametric modulator as 1. Group level analyses were conducted using a fixed effects model. Resulting images were cluster corrected (Z>2.3) to a corrected cluster significance threshold of p<0.05 (Worsley, 2001).

Conjunction analysis

We ran a GLM with one regressor each for accurate CC, SR, No Cue, and Invalid Cue trials, and nuisance regressors for inaccurate trials of each type. We then separately contrasted CC, SR, and No Cue trials with the implicit baseline. Using randomise, FSL's tool for nonparametric permutation testing, we conducted voxel-based correction for multiple comparisons to identify regions that were significantly active in each of the three contrasts (Winkler et al., 2014).

To test for significant activity in *multiple* contrasts, we performed a conjunction test for the null hypothesis (Nichols et al., 2005) analysis, taking the maximum values from these p value maps. Using this analysis, we determine regions that were significantly active in two (CC and SR, Table S1) or all three (CC, SR, and No Cue; Table 2) conditions.

Individual differences

The GLM was run as described in "Conjunction analysis". We then contrasted responses from pairs of cue types (CC v No Cue, SR v No Cue, CC v SR) and derived t-values for each voxel. Per participant, we extracted the t-values from voxels in each ROI and averaged them to gain an index of cue-specific responses within each ROI.

Supplemental References

Chun, M.M., and Jiang, Y. (2003). Implicit, long-term spatial contextual memory. J Exp Psychol Learn Mem Cogn *29*, 224-234.

Dinstein, I., Heeger, D.J., Lorenzi, L., Minshew, N.J., Malach, R., and Behrmann, M. (2012). Unreliable evoked responses in autism. Neuron *75*, 981-991.

Giesbrecht, B., Sy, J.L., and Guerin, S.A. (2013). Both memory and attention systems contribute to visual search for targets cued by implicitly learned context. Vision Res *85*, 80-89.

Greene, A.J., Gross, W.L., Elsinger, C.L., and Rao, S.M. (2007). Hippocampal differentiation without recognition: an fMRI analysis of the contextual cueing task. Learn Mem *14*, 548-553.

Greve, D.N., and Fischl, B. (2009). Accurate and robust brain image alignment using boundary-based registration. Neuroimage *48*, 63-72.

Grinband, J., Wager, T.D., Lindquist, M., Ferrera, V.P., and Hirsch, J. (2008). Detection of time-varying signals in event-related fMRI designs. Neuroimage *43*, 509-520.

Hagberg, G.E., Zito, G., Patria, F., and Sanes, J.N. (2001). Improved detection of event-related functional MRI signals using probability functions. Neuroimage *14*, 1193-1205.

Kasper, R.W., Grafton, S.T., Eckstein, M.P., and Giesbrecht, B. (2015). Multimodal neuroimaging evidence linking memory and attention systems during visual search cued by context. Ann N Y Acad Sci.

Nichols, T., Brett, M., Andersson, J., Wager, T., and Poline, J.B. (2005). Valid conjunction inference with the minimum statistic. Neuroimage *25*, 653-660.

Patenaude, B., Smith, S.M., Kennedy, D.N., and Jenkinson, M. (2011). A Bayesian model of shape and appearance for subcortical brain segmentation. Neuroimage *56*, 907-922.

Poldrack, R.A., and Packard, M.G. (2003). Competition among multiple memory systems: converging evidence from animal and human brain studies. Neuropsychologia *41*, 245-251.

Pruessner, J.C., Kirschbaum, C., Meinlschmid, G., and Hellhammer, D.H. (2003). Two formulas for computation of the area under the curve represent measures of total hormone concentration versus time-dependent change. Psychoneuroendocrinology *28*, 916-931.

Staresina, B.P., Duncan, K.D., and Davachi, L. (2011). Perirhinal and parahippocampal cortices differentially contribute to later recollection of object- and scene-related event details. J Neurosci *31*, 8739-8747.

Summerfield, J.J., Lepsien, J., Gitelman, D.R., Mesulam, M.M., and Nobre, A.C. (2006). Orienting attention based on long-term memory experience. Neuron *49*, 905-916.

Winkler, A.M., Ridgway, G.R., Webster, M.A., Smith, S.M., and Nichols, T.E. (2014). Permutation inference for the general linear model. Neuroimage *92*, 381-397.

Worsley, K.J. (2001). Statistical analysis of activation images. In Functional MRI: An Introduction to Methods, P. Jezzard, P.M. Matthews, and S.M. Smith, eds. (Oxford University Press).

Yin, H.H., and Knowlton, B.J. (2006). The role of the basal ganglia in habit formation. Nat Rev Neurosci *7*, 464-476.